Polymer-Templated Formation of Polydopamine-Coated SnO2 Nanocrystals: Anodes for Cyclable Lithium-Ion Batteries

Beibei Jiang, Yanjie He, Bo Li, Shiqiang Zhao, Shun Wang, Yan-Bing He, and Zhiqun Lin*

Abstract: *Well-controlled nanostructures and a high fraction of Sn/Li$_2$O interface are critical to enhance the coulombic efficiency and cyclic performance of SnO$_2$-based electrodes for lithium-ion batteries (LIBs). Polydopamine (PDA)-coated SnO$_2$ nanocrystals, composed of hundreds of PDA-coated "corn-like" SnO$_2$ nanoparticles (diameter ca. 5 nm) decorated along a "cob", addressed the irreversibility issue of SnO$_2$-based electrodes. The PDA-coated SnO$_2$ were crafted by capitalizing on rationally designed bottlebrush-like hydroxypropyl cellulose-graft-poly (acrylic acid) (HPC-g-PAA) as a template and was coated with PDA to construct a passivating solid-electrolyte interphase (SEI) layer. In combination, the corn-like nanostructure and the protective PDA coating contributed to a PDA-coated SnO$_2$ electrode with excellent rate capability, superior long-term stability over 300 cycles, and high Sn→SnO$_2$ reversibility.*

$\mathbf{S}$nO$_2$ has shown great potential as a substitute for graphite anodes because of its numerous appealing features; including abundance, environmental benignity, safe working potential, and high theoretical capacity.[1] The electrochemical interaction between Li and SnO$_2$ can be described in two steps, as shown below [Eqs. (1)–(2)].[2]

$$\mathrm{SnO_2 + 4Li^+ + 4e^- \rightarrow Sn + 2Li_2O} \tag{1}$$

$$\mathrm{Sn + xLi^+ + xe^- \leftrightarrow Li_xSn}\ (0 \leq x \leq 4.4) \tag{2}$$

It is widely recognized that conversion from Sn to SnO$_2$ (Equation (1)) is irreversible for bulk SnO$_2$ but can be reversible for nanostructured SnO$_2$.[2a,3] In contrast, Equation (2) is reversible, with a maximum uptake of 4.4 moles of Li ions per unit of Sn. Assuming Equation (1) to be fully irreversible, the commonly reported theoretical capacity is 782 mAh g^{-1}.[4] On the other hand, when considering both reactions to be completely reversible, the theoretical capacity

of 1494 mAh g^{-1} can be obtained (that is, a Li ion uptake of 8.4 moles).[5]

SnO$_2$ anodes experience a 358% volume change after lithiation.[6] Such a large volume change leads to mechanical failure and loss of electrical contact.[3b,4a] Additionally, the formed active Sn nanoparticles have a strong tendency to aggregate into big and inactive Sn clusters even at room temperature.[7] Moreover, the large volume change can easily break the SEI layer and expose the fresh surface of active materials to electrolyte, leading to continuous growth of the SEI layer. Taken together, severe capacity fading in SnO$_2$-based electrodes is often observed.[5]

In this context, much effort has been directed toward constructing nanostructured SnO$_2$.[4b,8] Nanostructured materials carry many advantages, such as better accommodation of volume change,[9] reduced transport length for lithium ions and electrons, a high electrode/electrolyte contact area favorable for improving the lithium reaction rate, and a large volume fraction of Sn/Li$_2$O interfaces that are beneficial for Sn to SnO$_2$ conversion.[2a,10] However, the use of nanostructured SnO$_2$ alone is not sufficient to significantly enhance cycling stability, as SnO$_2$ nanomaterials and the produced Sn nanoparticles will still easily aggregate.[11] On the other hand, the ability to form a passivating SEI layer is critical for realizing high reversibility and long-term cycling stability.[12] Thus, nanostructured SnO$_2$ with a high Sn→SnO$_2$ reversibility, suppressed Sn aggregation, and a stable SEI layer during cycling, would be an ideal material for realizing high-performance LIBs.

Herein, polydopamine (PDA)-coated corn-on-the-cob-like SnO$_2$ nanocrystals (denoted PDA-coated SnO$_2$) comprising SnO$_2$ nanoparticles (diameter ca. 5 nm) decorated along a "cob" was crafted as an electrode. Specifically, PDA-coated SnO$_2$ was created with the aid of a hydrophilic bottlebrush-like hydroxypropyl cellulose-*graft*-poly(acrylic acid) template (denoted HPC-*g*-PAA), as depicted by Figure 1. Hydroxypropyl cellulose (HPC) was first converted into HPC-based macroinitiator (that is, HPC-Br) by homogeneous esterification. The nearly 100% esterification efficiency (Supporting Information, Figure S1) indicates that all hydroxyl groups on HPC were converted into active Br-terminated groups. The poly(*tert*-butyl acrylate) (P*t*BA) blocks were then grafted onto HPC-Br by atom transfer radical polymerization (ATRP), yielding HPC-*g*-P*t*BA. The hydrolysis of P*t*BA into PAA produced hydrophilic bottlebrush-like HPC-*g*-PAA, which served as the template for growing SnO$_2$ nanocrystals. The instantly formed SnO$_2$ nanoparticles were quickly bonded to PAA blocks of HPC-*g*-PAA because of the strong coordinative interaction between the -COOH groups of PAA blocks and SnO$_2$ nanoparticles,[13] yielding a nano-

[*] B. Jiang, Y. He, B. Li, S. Zhao, Prof. Z. Lin
School of Materials Science and Engineering
Georgia Institute of Technology
Atlanta, GA 30332 (USA)
E-mail: zhiqun.lin@mse.gatech.edu

Prof. S. Wang
College of Chemistry and Materials Engineering, Wenzhou University
Wenzhou, Zhejiang, 325035 (P.R. China)

Prof. Y. He
Engineering Laboratory for the Next Generation Power and Energy
Storage Batteries, Graduate School at Shenzhen, Tsinghua University
Shenzhen, Guangdong, 518055 (P.R. China)

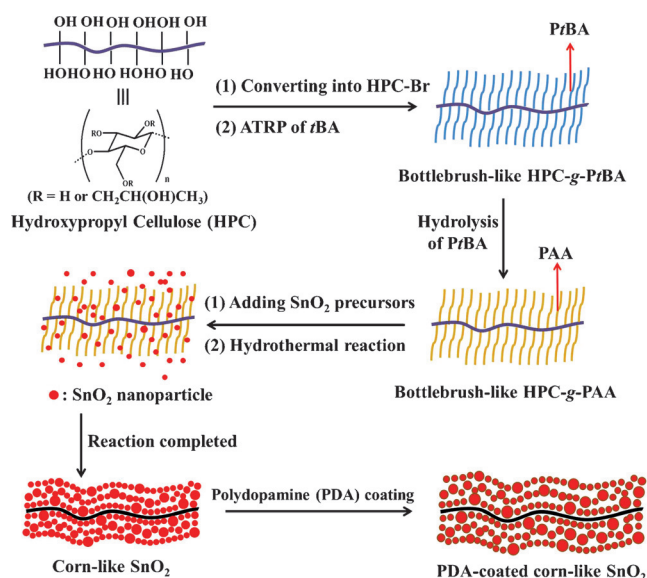Supporting information for this article can be found under:
http://dx.doi.org/10.1002/anie.201611160.

Figure 1. Synthesis of the hydrophilic bottlebrush-like HPC-*g*-PAA polymer template and templated growth of PDA-coated corn-like SnO$_2$ nanocrystals.

Figure 2. a,b) Lower magnification and c,d) higher magnification TEM images of PDA-coated SnO$_2$ nanocrystals. Key (d): crystalline SnO$_2$ nanoparticles (solid circles), pores (dashed circles), PDA coating (arrows).

structure resembling a corn-on-the-cob. Finally, each SnO$_2$ nanoparticle was coated with a thin layer of PDA by simple polymerization of dopamine,[14] forming PDA-coated SnO$_2$ nanocrystals (lower right panel in Figure 1). Fourier transform infrared spectroscopy (FTIR) confirmed successful coating of PDA (Supporting Information, Figure S2).

Small SnO$_2$ nanoparticles (solid circles in Figure 2 d) with an average size of approximately 5 nm are bonded along the bottlebrush-like HPC-*g*-PAA template, forming a corn-like structure (Figure 2 c,d). The voids of 3–5 nm between SnO$_2$ nanoparticles were clearly seen (dashed circles in Figure 2 d). To corroborate the role of bottlebrush-like HPC-*g*-PAA in guiding the formation of SnO$_2$, three control experiments were also performed (Supporting Information, Table S1 and TEM images in Figure S3).

The X-ray diffraction (XRD) patterns are shown in Figure S4 (Supporting Information). All peaks can be assigned to the tetragonal rutile-like SnO$_2$.[5] The calculated SnO$_2$ sizes are summarized in Table S2 (Supporting Information). The surface structure and porosity of the samples were investigated by N$_2$-sorption measurements (Supporting Information, Figure S5 a–c and Table S2). All samples exhibited a type IV isotherm curve with a small hysteresis loop, suggesting the presence of a mesoporous structure.

Figure 3 a shows the cyclic voltammetry (CV) characteristics for the PDA-coated SnO$_2$ electrode. For initial discharge the broad peak in the range of 0.8 to 1.2 V is due to the formation of SEI layers and the conversion of SnO$_2$ to Sn and Li$_2$O.[5,15] The weak peak at approximately 0.2 V can be assigned to the alloying reaction between Sn and Li ions.[16] In the first charge process the sharp peak at 0.58 V corresponds to the reversible Li$_x$Sn dealloying reaction, while the weaker and broader peak at 1.27 V is attributed to the conversion from Sn to SnO$_2$.[5,16a] For the following cycles the broad cathodic peaks in the range of 0.8 to 1.2 V shift to the lower
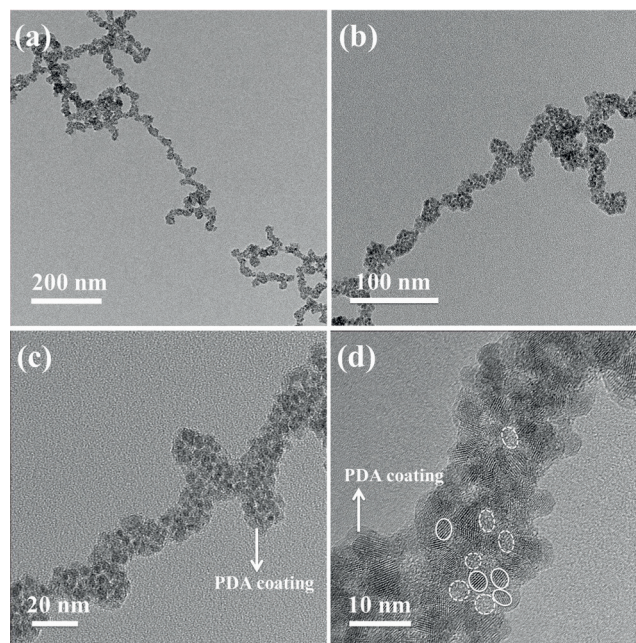
voltage with cycling, which was assigned to the conversion of SnO$_2$→SnO→Sn.[15] Moreover, the cathodic peak at around 0.2 V becomes more significant during cycling. Additionally, all the peak currents (also capacities in mA h) for later cycles are higher than the previous cycles, suggesting an activated electrochemical process.

Figure 3 b depicts the charge–discharge profiles of the PDA-coated SnO$_2$ electrode. The initial coulombic efficiency is approximately 61.3% (945/1542 = 61.3%), larger than 52.3% (782/1494 = 52.3%), which is the largest initial coulombic efficiency calculated if Equation (1) is assumed to be completely irreversible after initial discharge; this signifies that the widely assumed irreversible conversion from Sn to SnO$_2$ is at least partially reversible for this PDA-coated SnO$_2$ electrode.

The cycling performance at 160 mA g^{-1} is shown in Figure 3 c. For the uncoated SnO$_2$ electrode, the capacity displays a good cyclability for the first 150 cycles, reaches the highest value at the 150th cycle, and continuously decays after 150 cycles. In sharp contrast, the PDA-coated SnO$_2$ exhibits significantly improved cycling stability and demonstrates a much higher capacity for the entire cycle life, which may be attributed to the combined effects of the corn-like nanostructures and the PDA coating. The PDA-coated CS3 anode that was templated by linear PAA and possessed a similar corn-like structure displays a good cycling stability, superior to that of PDA-coated CS2 anode that was formed in the absence of polymer template (Figure 3 d). However, because of the limited mass loading of active SnO$_2$ in PDA-coated CS3 (45 wt% in PDA-coated CS3, 84 wt% in PDA-coated SnO$_2$; Supporting Information, Figure S6), the specific capacities calculated based on the total mass are
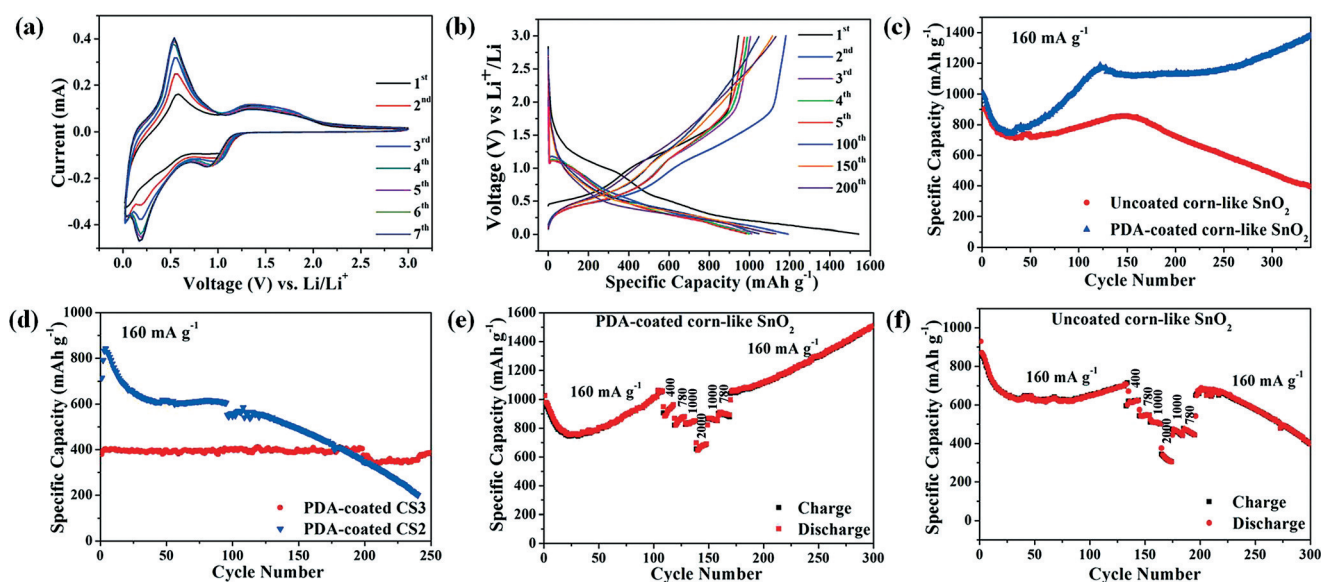
Figure 3. a) CV curves of the first seven cycles for the fresh cell based on a PDA-coated SnO_2 electrode tested at 0.1 mV s^{-1} in the range of 0.005–3 V. b) Galvanostatic charge–discharge voltage profiles for the first five cycles, 100th, 150th, and 200th cycles of the PDA-coated SnO_2 electrode tested at 160 mA g^{-1} in the range of 0.01–3.0 V vs. Li/Li$^+$. Cycling performance tested at 160 mA g^{-1} for c) PDA-coated and uncoated SnO_2 electrodes, and d) PDA-coated CS3 and CS2, in which CS3 and CS2 were formed using linear PAA as a template and in the absence of a polymer template, respectively. Rate performance for e) PDA-coated SnO_2 electrode and f) uncoated SnO_2 electrode.

much lower. Nonetheless, the markedly improved cycling performance of the SnO_2 electrodes indicates that the combination of the nanostructured morphology and a protective PDA coating promotes reversible conversion from Sn to SnO_2 and imparts long-term cycling stability to the SnO_2-based anodes.

Figure 3e,f compares the rate performance of PDA-coated and uncoated SnO_2 electrodes. The LIBs were first cycled at 160 mA g^{-1}, followed by testing at various current densities, and then were back-cycled at 160 mA g^{-1} to investigate any structural changes caused by previous rate testing. For the PDA-coated SnO_2 electrode the average capacities are 921, 851, 835, and 667 mA h g^{-1} at 400, 780, 1000, and 2000 mA g^{-1}, respectively (see closes-ups in the Supporting Information, Figure S7a). When the current density returns to 160 mA g^{-1} the high capacity is resumed and continues to rise over cycling; it is positioned at 1502 mA h g^{-1} at the 300th cycling, implying an activated electrochemical process.[2a,17] For the uncoated SnO_2 (Figure 3 f), however, the capacity decays quickly over cycling and fails to return to previously high values when back-cycled, indicating that the cyclability is largely disrupted by the rate testing. The superior cyclability of PDA-coated SnO_2 electrode is further manifested in the cycling performance at various current densities of 200, 400, 780, and 1500 mA g^{-1} for over 300 cycles (Supporting Information, Figure S8a–d). This data further indicates that the PDA coating is beneficial to maintaining cycling stability and reversibility of SnO_2 electrodes; probably because the PDA coating suppresses Sn coarsening and retains a large Sn/Li$_2$O interface that facilitates the reversible reaction between Sn and Li$_2$O.

Figure S9a,b (Supporting Information) compares the electrochemical impedance spectroscopy (EIS) Nyquist plots of the freshly assembled catalyst, and after the 1st,

2nd, 100th, and 300th cycles. For the PDA-coated SnO_2, the R_{ohm} after the 300th cycle is similar to that after the 100th cycle. However, R_{ohm} for uncoated SnO_2 after the 300th cycle increases significantly compared with that after the 100th cycle, indicating the formation of thick SEI films. Clearly, the PDA coating provides an elastic buffer for accommodating the volume change of active materials and prevents their direct contact with the electrolyte. Thus, continuous depletion of electrolyte is prevented and the long-term stability of the SEI film is maintained.

The batteries were dissembled in a glove box after cycling and characterized by ex situ scanning electron microscopy (SEM) and X-ray photoelectron spectroscopy (XPS). As shown in Figure 4, thick SEI films are clearly evident for the uncoated SnO_2 electrode (Figure 4c,d), while the SEI film is much thinner and the morphology remains almost unchanged for the PDA-coated SnO_2 electrode (Figure 4e,f), signifying the protective function of the PDA coating. The protective PDA layer combined with the corn-like nanostructure accounts for the observed superior cyclability of the PDA-coated SnO_2 electrode.

The XPS spectrum (Supporting Information, Figure S10) for the PDA-coated SnO_2 electrode after cycling exhibits the same binding energy as the as-prepared electrode with two broad peaks centered at 495.6 and 487.2 eV. These two peaks can be assigned to Sn 3d$_{3/2}$ and Sn 3d$_{5/2}$, respectively, corresponding to Sn^{4+} in SnO_2,[11,18] indicating that conversion from Sn to SnO_2 [Eq. (1)] is reversible for the PDA-coated SnO_2. However, for the uncoated SnO_2 electrode after cycling the peaks shift to lower binding energies, which can be attributed to the formation of SnO.[11,19] This comparison confirmed that the PDA coating is helpful for reversible conversion from Sn to SnO_2 [Eq. (1)].
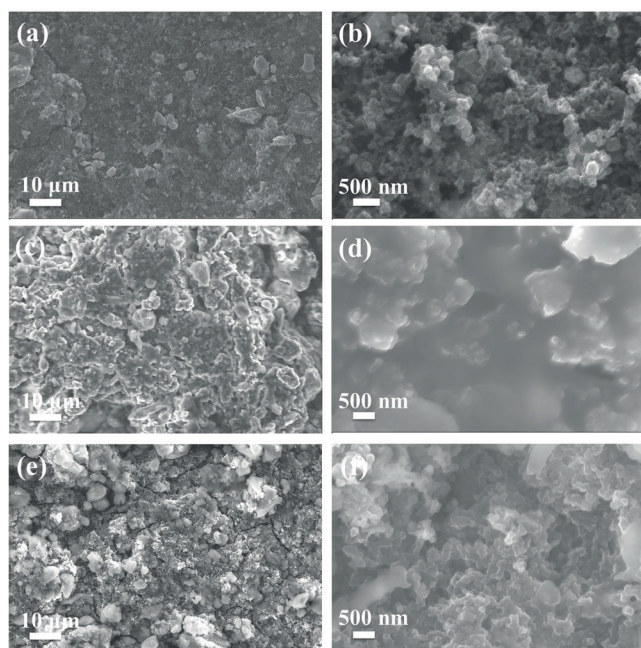
Figure 4. SEM images: a,b) freshly prepared electrode at different magnifications; c,d) uncoated SnO₂ electrode after cycling at 160 mA g⁻¹ for 300 cycles; e,f) PDA-coated SnO₂ electrode after cycling at 160 mA g⁻¹ for 300 cycles.

In summary, we crafted corn-like PDA-coated SnO₂ nanocrystals using a HPC-*g*-PAA template. Batteries based on uncoated SnO₂ demonstrated a good short-term cycling stability for 150 cycles and a good rate performance (attributed to shortened transport length), good structural stability, high porosity, and limited aggregation of Sn nanoparticles, which was endowed by the corn-like nanostructure. Moreover, the introduction of a protective PDA coating contributed to the construction of a passivating SEI layer. In combination, the corn-like nanostructure and the protective PDA coating enabled excellent electrochemical performance of the SnO₂ electrode; including, superior long-term cycling stability for over 300 cycles, high Sn→SnO₂ reversibility, and excellent rate capability. The bottlebrush-like polymer templating strategy is facile and robust; thus, we envisage that this technique can be readily extended to create a rich variety of functional metal oxides and metal sulfides for high-performance LIBs.

Acknowledgements

Conflict of interest

The authors declare no conflict of interest.

[1] X. W. Lou, Y. Wang, C. Yuan, J. Y. Lee, L. A. Archer, *Adv. Mater.* **2006**, *18*, 2325–2329.

[2] a) R. Hu, D. Chen, G. Waller, Y. Ouyang, Y. Chen, B. Zhao, B. Rainwater, C. Yang, M. Zhu, M. Liu, *Energy Environ. Sci.* **2016**, *9*, 595–603; b) R. Retoux, T. Brousse, D. M. Schleich, *J. Electrochem. Soc.* **1999**, *146*, 2472–2476.

[3] a) X. W. Lou, J. S. Chen, P. Chen, L. A. Archer, *Chem. Mater.* **2009**, *21*, 2868–2874; b) C.-M. Wang, W. Xu, J. Liu, J.-G. Zhang, L. V. Saraf, B. W. Arey, D. Choi, Z.-G. Yang, J. Xiao, S. Thevuthasan, D. R. Baer, *Nano Lett.* **2011**, *11*, 1874–1880.

[4] a) Y. Yu, C. H. Chen, Y. Shi, *Adv. Mater.* **2007**, *19*, 993–997; b) D. Deng, J. Y. Lee, *Chem. Mater.* **2008**, *20*, 1841–1846.

[5] X. Zhou, L.-J. Wan, Y.-G. Guo, *Adv. Mater.* **2013**, *25*, 2152–2157.

[6] L. Y. Beaulieu, K. W. Eberman, R. L. Turner, L. J. Krause, J. R. Dahn, *Electrochem. Solid-State Lett.* **2001**, *4*, A137–A140.

[7] I. A. Courtney, W. R. McKinnon, J. R. Dahn, *J. Electrochem. Soc.* **1999**, *146*, 59–68.

[8] a) N. Zhao, G. Wang, Y. Huang, B. Wang, B. Yao, Y. Wu, *Chem. Mater.* **2008**, *20*, 2612–2614; b) S. M. Paek, E. Yoo, I. Honma, *Nano Lett.* **2009**, *9*, 72–75.

[9] a) J. O. Besenhard, J. Yang, M. Winter, *J. Power Sources* **1997**, *68*, 87–90; b) H. Wu, G. Chan, J. W. Choi, I. Ryu, Y. Yao, M. T. McDowell, S. W. Lee, A. Jackson, Y. Yang, L. Hu, Y. Cui, *Nat. Nanotechnol.* **2012**, *7*, 310–315.

[10] B. Jiang, C. Han, B. Li, Y. He, Z. Lin, *ACS Nano* **2016**, *10*, 2728–2735.

[11] M. He, L. Yuan, X. Hu, W. Zhang, J. Shu, Y. Huang, *Nanoscale* **2013**, *5*, 3298–3305.

[12] a) D. Deng, M. G. Kim, J. Y. Lee, J. Cho, *Energy Environ. Sci.* **2009**, *2*, 818–837; b) R. Marom, S. F. Amalraj, N. Leifer, D. Jacob, D. Aurbach, *J. Mater. Chem.* **2011**, *21*, 9938–9954.

[13] a) B. Jiang, X. Pang, B. Li, Z. Lin, *J. Am. Chem. Soc.* **2015**, *137*, 11760–11767; b) L. Zhang, G. Zhang, H. B. Wu, L. Yu, X. W. Lou, *Adv. Mater.* **2013**, *25*, 2589–2593; c) X. Pang, Y. He, J. Jung, Z. Lin, *Science* **2016**, *353*, 1268–1272.

[14] J. Liebscher, R. Mrówczyński, H. A. Scheidt, C. Filip, N. D. Hădade, R. Turcu, A. Bende, S. Beck, *Langmuir* **2013**, *29*, 10539–10548.

[15] K. Shiva, H. Rajendra, K. Subrahmanyam, A. J. Bhattacharyya, C. Rao, *Chem. Eur. J.* **2012**, *18*, 4489–4494.

[16] a) R. Demir-Cakan, Y.-S. Hu, M. Antonietti, J. Maier, M.-M. Titirici, *Chem. Mater.* **2008**, *20*, 1227–1229; b) L. Liu, M. An, P. Yang, J. Zhang, *Sci. Rep.* **2015**, *5*, 9055.

[17] C. Guan, X. Wang, Q. Zhang, Z. Fan, H. Zhang, H. J. Fan, *Nano Lett.* **2014**, *14*, 4852–4858.

[18] X. Wang, X. Cao, L. Bourgeois, H. Guan, S. Chen, Y. Zhong, D. M. Tang, H. Li, T. Zhai, L. Li, *Adv. Funct. Mater.* **2012**, *22*, 2682–2690.

[19] J.-Y. Jung, S.-B. Lee, H.-Y. Lee, Y.-C. Joo, Y.-B. Park, *J. Electron. Mater.* **2009**, *38*, 691–699.